THE JOURNAL OF PHYSICAL CHEMISTRY C

Article

pubs.acs.org/JPCC

$CoFe_2O_4$ Nanoparticle-Integrated Spin-Valve Thin Films Prepared by Interfacial Self-Assembly

Chengpeng Jiang,[†] Ping Hoi Chan,[†] Chi Wah Leung,[‡] and Philip W. T. Pong*[,†]

[†]Department of Electrical and Electronic Engineering, The University of Hong Kong, Hong Kong

[‡]Department of Applied Physics, Hong Kong Polytechnic University, Hong Kong

Supporting Information

ABSTRACT: We report the fabrication of nanoparticle-integrated spin-valve system and investigate its magnetic properties and magnetotransport behaviors. Using a modified interfacial self-assembly method, chemically synthesized $CoFe_2O_4$ nanoparticles were assembled as a Langmuir film on liquid/air interface. This film was further deposited on the sputtered thin films of bottom-pinned spin valve without additional treatment. The nanoparticle-assembled film with multilayer structure exhibits uniform and compact surfaces. Magnetization and magnetoresistance study show that the integrated nanoparticles give rise to a reduced interlayer coupling field and an increased magnetoresistance (MR) ratio in the spin valve. By analyzing the magnetic interaction between the nanoparticles and the spin valve, it is inferred that the magnetic stray field induced by the single-domain magnetic nanoparticles reduces the external magnetic field on the free layer, leading to the change of free-layer magnetization and the attenuation of interlayer coupling. The decrease of this ferromagnetic-type interlayer coupling resulted in a more favorable antiparallel magnetization configuration, manifested by the enhancement of MR ratio. This work demonstrates the integration of self-assembled nanoparticles with exchange-biased thin films, and the results suggest that nanoparticle integration can be employed as an alternative route to modulate the magnetization switching and magnetoresistance of spin valves.

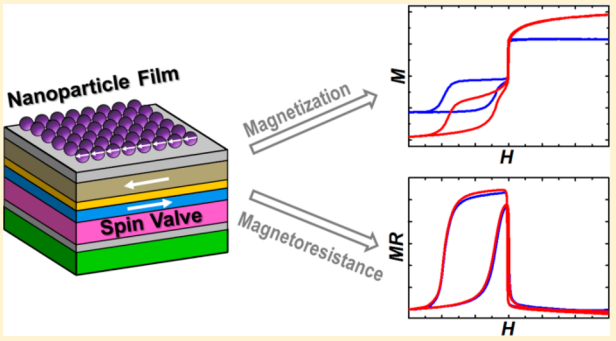

1. INTRODUCTION

Spin-valve devices have been widely researched not only due to the fundamental physics of spin transport in their magnetic nanostructures but also the great potential they demonstrate in magnetic recording, storage, and sensing applications.[1,2] The standard spin valve consists of two ferromagnetic (FM) layers separated by a nonmagnetic spacer and an antiferromagnetic (AF) layer to pin the magnetization of one FM layer by exchange-bias effect.[3] Early works about spin valves fabricated as giant magnetoresistance (GMR) multilayers mostly focused on the materials and growth of magnetic layers (disordered and ordered AF materials,[4,5] crystalline and amorphous FM materials[6,7]), treatment and processing (magnetic annealing,[8] rapid annealing,[9] oxidation[10,11]), and structural modification (current-perpendicular-to-plane geometry,[12,13] synthetic antiferromagnets,[14,15] dual spin valve,[13,16] lateral spin valve[17,18]),[19] leading to the improvement of sensitivity, areal density, magnetoresistance (MR) ratio, exchange-bias field, and so forth. Later on, wide-band gap metal oxides, mainly MgO and Al_2O_3, have been used as the tunnel barrier in spin valves and pseudo spin valves deposited as tunneling magnetoresistance (TMR) multilayers, achieving significantly higher MR ratios.[20−22] Most recently, atomically thin 2D materials, such as graphene,[23,24] boron nitride,[25] and transition-metal dichalcogenides,[26] were exploited to be used as the spacer layer in organic spin valves, generating considerable TMR signals with good stability.[27−29] Despite these research works, modifying the properties of spin valve using magnetic nanoparticles (Fe_3O_4, $CoFe_2O_4$, FePt)[30] have been rarely attempted. It is of fundamental value and practical interest if magnetic nanoparticles can be appropriately integrated in the active region or on the surface of spin-valve thin films.[31−35] This is due to the following: first, magnetic nanoparticles with various morphologies and different compositions can be obtained in a cost-effective manner by chemical routes;[30,36] second, magnetic nanoparticles with monodisperse size usually possess an intrinsic insulating layer of stabilizing ligands and additional material interface/surface,[37,38] providing favorable sites for spin-dependent tunneling and scattering;[33,39] and third, magnetic nanoparticles exhibiting superparamagnetic and single-domain properties[40] are expected to tune the magnetization and magnetotransport behaviors of spin valve through magnetic interactions.

The major challenge of integrating magnetic nanoparticles with spin valve is the controlled assembly of nanoparticles as uniform structures.[41] Several methods, such as drying-mediated

Received: July 22, 2017
Revised: September 18, 2017
Published: September 18, 2017

DOI: 10.1021/acs.jpcc.7b07242
J. Phys. Chem. C 2017, 121, 22508−22516

(or evaporation-induced) self-assembly,[42,43] chemically assisted self-assembly,[44,45] and interfacial self-assembly,[38,46−49] have been employed to construct magnetic nanoparticles as layered coatings, defined patterns, or hierarchical superstructures under the guidance of field or template.[50,51] Nevertheless, commonly adopted nanoparticle self-assembly strategies require chemical functionalization or heat treatment of the substrates, which in turn will deteriorate the performance of spin valve, considering its corrosion resistance and thermal stability.[4,52] In this regard, a suitable method for nanoparticle assembly on magnetic thin films needs to be developed for the purpose of fabricating nanoparticle-integrated spintronic devices and investigating their physical properties.

Herein, this work demonstrates the facile fabrication of magnetic-nanoparticle-integrated spin-valve system. The nanoparticles were $CoFe_2O_4$ nanoparticles with small size but high saturation magnetization. Nanoparticle-assembled film was prepared at liquid/air interface by a modified interfacial self-assembly method. Surface morphology and nanoparticle arrangement of the assembled structure were characterized at different scales. Magnetization and magnetoresistance study of the nanoparticle-integrated spin valve were further performed to investigate the influence of nanoparticle integration on the magnetic properties and magnetotransport behaviors of the spin valve. Magnetic interaction between the nanoparticle and the spin valve was analyzed by considering exchange-bias effect, interlayer coupling, free-layer magnetization, and the stray field generated from the nanoparticles.

2. EXPERIMENTAL SECTION

2.1. Synthesis of Nanoparticles. $CoFe_2O_4$ nanoparticles were synthesized following a literature protocol with several modifications.[53] $Fe(acac)_3$ (2 mmol), $Co(acac)_3$ (1 mmol), 1,2-tetradecanediol (10 mmol), oleic acid (6 mmol), oleylamine (6 mmol), and benzyl ether (20 mL) were mixed and degassed for 30 min in a three-neck flask equipped with a condenser. Under a nitrogen blanket, the reaction mixture was heated to 200 °C for 1.5 h (ramp 10 °C min^{-1}) and then heated to reflux (~290 °C) for 1 h (ramp 5 °C min^{-1}). The black mixture was cooled to room temperature and then purified by precipitating and dissolving operations using acetone and chloroform solvent (3:1). This purification procedure was repeated three times to remove excessive surfactants. The solid products were redispersed in 12 mL of toluene and then centrifuged to remove any undissolved materials, producing a highly stable solution of surfactant-coated nanoparticles with a concentration of 18 mg mL^{-1}.

2.2. Preparation of Nanoparticle-Assembled Film on Si Substrate. Nanoparticle-assembled film on Si substrate was prepared through an improved interfacial self-assembly method.[46] As schematically illustrated in Figure 1a, Milli-Q water was filled into a glass Petri dish (diameter 5 cm), and a square Si/SiO_2 substrate (size 1 cm; thermally oxidized surface) was fully immersed into the water using a substrate holder. The substrate was tilted at 20° to define the assembly direction. Toluene solution of the $CoFe_2O_4$ nanoparticles (17.5 μL) was then dropped onto the water surface at a height of 3 cm using a micropipet. The black-brown solution quickly spread over the water surface, producing a thin liquid layer supported on water surface. A glass lid was partially covered above this liquid layer to control its evaporation rate. As the toluene evaporated (~2 min), nanoparticles were assembled onto the liquid/air interface, leading to a floating film on water surface.

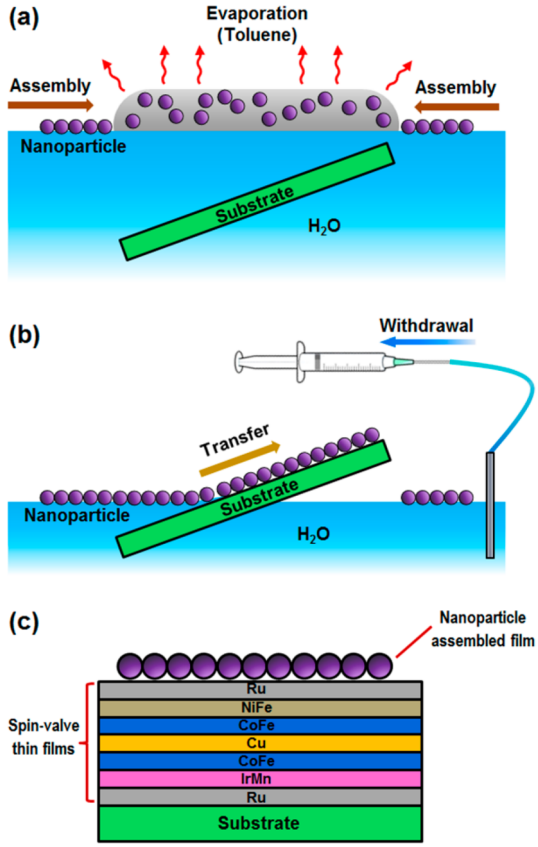

Figure 1. (a) Self-assembly of $CoFe_2O_4$ nanoparticles on liquid/air interface. (b) Transferring the nanoparticle-assembled film to substrate surface. (c) Schematic illustration of the nanoparticle-integrated spin-valve thin films. Not to scale.

Subsequently, as illustrated in Figure 1b, the underneath water was withdrawn using a syringe pump to transfer the floating film onto the substrate surface (speed 2 mm min^{-1}). Finally, the obtained solid film on Si was allowed to dry for additional 10 min.

2.3. Preparation of Nanoparticle-Assembled Film on Spin Valve. Bottom-pinned spin valve was first fabricated on Si/SiO_2 substrate using a magnetron sputtering system (AJA). The base pressure was 9×10^{-9} Torr and the deposition operations were performed in argon atmosphere at a pressure of 3 mTorr. The spin valve possessed the structure of substrate/Ru (3.5 nm)/$Ir_{20}Mn_{80}$ (9 nm)/$Co_{50}Fe_{50}$ (3.4 nm)/Cu (4 nm)/$Co_{50}Fe_{50}$ (0.5 nm)/$Ni_{80}Fe_{20}$ (7 nm)/Ru (3 nm). During the sputtering process, an in-plane magnetic field of 400 Oe was applied to induce the exchange anisotropy and magnetic anisotropy directions. The spin valve was further annealed in vacuum (10^{-6} Torr) at 210 °C for 0.5 h under an in-plane magnetic field of 1.6 kOe to enhance the exchange-bias effect and unidirectional magnetic anisotropy. Finally, nanoparticle-integrated spin valve was prepared by depositing the nanoparticle-assembled film on the surface of spin valve using the interfacial self-assembly method as mentioned above. The structure of the nanoparticle-integrated spin-valve thin films is presented in Figure 1c.

2.4. Characterizations. The nanoparticles were analyzed by transmission electron microscopy (TEM, FEI Tecnai-G2), X-ray diffraction (XRD, Rigaku SmartLab), and vibrating sample magnetometer (VSM, MicroSense). The nanoparticle-assembled films were characterized by optical microscopy

DOI: 10.1021/acs.jpcc.7b07242
J. Phys. Chem. C 2017, 121, 22508−22516

(Olympus BX-51), scanning electron microscopy (SEM, LEO 1530), and atomic force microscopy (AFM, Digital Instruments NanoScope-IV). Magnetization curves were acquired by VSM. Magnetoresistance curves were obtained by four-point-probe method. The four probes were configured in linear arrangement and placed perpendicular to the applied field direction to make the effect of anisotropic magnetoresistance (AMR) negligible.[54] The magnetization and magnetoresistance measurements were both performed at room temperature with the applied field parallel to the easy-axis direction of the spin valve, and the measurements were repeated three times to remove training effects.[55,56]

3. RESULTS AND DISCUSSION

3.1. Cobalt Ferrite Nanoparticles. A prerequisite for nanoparticle assembly is the preparation of highly stable organic solution of uniform nanoparticles. Cobalt ferrite nanoparticles capped by organic surfactants were synthesized by thermal decomposition of organometallic precursors.[57] Benzyl ether was used as the reaction solvent to promote the anisotropic growth of single-crystalline nanoparticles.[58,59] Oleic acid and oleylamine were used as surfactants to stabilize the nanoparticles and prevent them from agglomeration.[42] It has been commonly reported that the heating profile has pronounced effects on nanoparticle morphology.[36,40,60] Therefore, the heating rate and the heating time were optimized to reduce the size distribution of nanoparticles. The nanoparticle size was controlled under 10 nm, because small-sized magnetic nanoparticles exhibit low coercivity and single-domain behavior, which are favorable for nanoparticle assembly and device integration.[40,61,62]

Morphology of the nanoparticles was investigated using TEM. By dropping the diluted nanoparticle solution (5 μL) onto carbon-coated TEM grids and controlling the evaporation rate of the solvent, the nanoparticles spontaneously organized into hexagonal (Figure 2a) and square (Figure 2b) packing patterns, corresponding to nanoparticle solution concentration of 1.2 and 2.4 mg mL^{-1}, respectively. In these nanoparticle-assembled monolayers, the arrangement order indicates the uniformity of particle size and the structural diversity implies the shape-selective nature of the evaporation-induced self-assembly considering the faceted particle surface.[63−65] These polyhedral nanoparticles have a size of 9.8 ± 0.4 nm and a spacing of 1.4 ± 0.2 nm, as determined by TEM (Figure 2a). This spacing was induced by the surfactant coating capped on nanoparticle surface as a steric barrier.[42] Structural information on the nanoparticles was obtained from XRD. As shown in Figure 2c, the positions and relative intensities of all the diffraction peaks are well indexed to the standard diffraction data of $CoFe_2O_4$ with inverse spinel structure (JCPDS: 22-1086). Magnetic properties of the nanoparticles were studied using VSM. As shown in the hysteresis loop in Figure 2d, the saturation magnetization (M_s) and coercivity (H_c) of the nanoparticles in powder form are 77.1 ± 0.3 emu g^{-1} and 2.0 ± 0.1 Oe, respectively. The saturation magnetization of the $CoFe_2O_4$ nanoparticle is lower than the value of its bulk counterpart (93.9 emu g^{-1}) probably due to the synergistic results of canted spin structure, lattice strain effect, presence of nonmagnetic organics, and slight oxidation of nanoparticle surfaces.[66]

3.2. Nanoparticle-Assembled Film on Si. In general, the interfacial self-assembly method stands out as a simple and versatile strategy to build nanoparticles into monolayer or multilayer structures.[47,67−69] In this work, the hydrophobic nanoparticles capped by nonpolar surfactants were dispersed in toluene, and this nanoparticle solution was spread on water surface, producing a liquid/liquid interface between the immiscible aqueous and organic phases. With the evaporation of the upper liquid layer of toluene, the solid nanoparticles were readily formed into a floating film supported on water surface. The self-assembly process was driven by the minimization of surface tension and the nanoparticle organization was mainly determined by surfactant properties, particle morphologies, and self-assembly dynamics.[68] The Langmuir technique was employed to transfer the floating film to a desired substrate. By manipulating the water level using a syringe pump, the liquid/air contact line continuously swept the substrate surface. As the evaporation proceeded and the drying front moved, this floating film was deposited onto the substrate.[47,48]

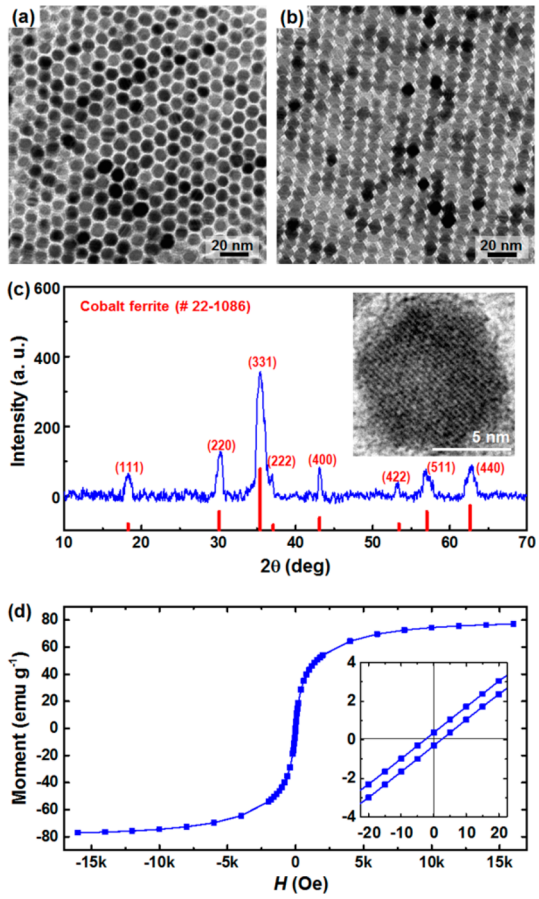

Figure 2. TEM images showing the spontaneous self-assembly of $CoFe_2O_4$ nanoparticles as (a) hexagonal and (b) cubic packing patterns. (c) XRD pattern (inset, high-resolution TEM) and (d) hysteresis loop (inset, enlarged part near the origin) of $CoFe_2O_4$ nanoparticles.

Nanoparticle-assembled film was first prepared on Si/SiO_2 substrate to explore the feasibility of transferring the Langmuir film of nanoparticles through lift-off. Surface characterization by optical microscopy (Figure S1a) and SEM (Figure S1b) reveal that the film has homogeneous surface with clear boundary and it is composed of closely packed nanoparticles. AFM analysis (Figure S1c) gives a root-mean-square roughness of 2.6 nm and a film thickness of 32.9 ± 1.0 nm, corresponding to three layers of nanoparticles. This nanoparticle-assembled film on Si/SiO_2 exhibits mechanical robustness and structural continuity,[46]

DOI: 10.1021/acs.jpcc.7b07242
J. Phys. Chem. C 2017, 121, 22508−22516

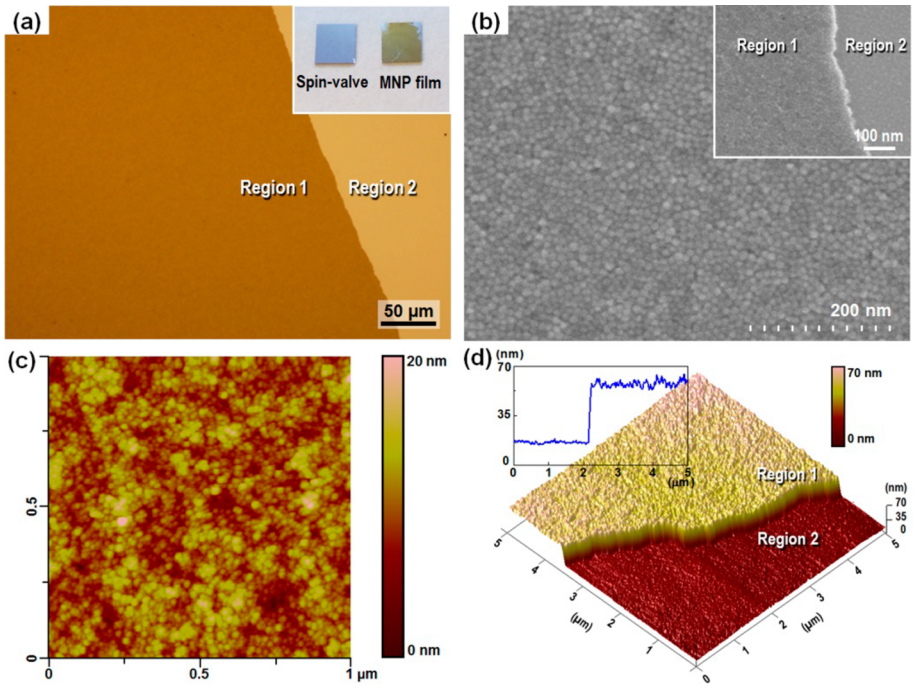

Figure 3. (a) Optical image (inset, photograph), (b) SEM image (inset, regions near the film boundary), and (c) AFM image of the $CoFe_2O_4$ nanoparticle-assembled film on spin-valve thin films. (d) A 3D AFM image taken at the film boundary (inset: cross-section profile). Region 1 represents magnetic nanoparticle film, while region 2 represents bare spin-valve surface.

allowing the investigation of collective magnetic behaviors of the self-assembled nanoparticles. Its direct transfer from liquid surface to solid substrate provides guidelines for the integration of magnetic nanoparticles with sputtered thin films.

3.3. Nanoparticle-Assembled Film on Spin Valve. Previous reports on the integration of magnetic nanoparticles with magnetic thin films include direct growth of thin films on ion-milled nanoparticles,[70] formation of ultrasmall nanoparticles in the barrier of magnetic tunneling junction (MTJ),[31] and analytical modeling of nanoparticle-embedded MTJ with double-barrier structure.[71] Earlier works on the interaction between spin valve and magnetic nanoparticles were related to nanoparticle detection and sensor optimization,[72−75] while the topic of utilizing self-assembled magnetic nanoparticles to modulate the performance of spin valve, to the best of our knowledge, has not been explored so far. In this work, nanoparticle-integrated spin-valve samples were prepared by fabricating the nanoparticle-assembled film on the sputtered thin films of spin valve. In the bottom-pinned spin-valve structure, the magnetization of the bottom FM layer was pinned by the AF layer, whereas the magnetization of the top FM layer was free to rotate with the external field. Thus, the stray field induced from the magnetic nanoparticles can effectively affect the magnetic orientation of the free layer, and discernible magnetic interactions between the nanoparticles and the free layer can be expected.[75] The first Ru layer was grown as a buffer to promote the (111) texture of IrMn and the last Ru layer serves as a capping to protect the underlying thin films against oxidation.[3] The thickness of the IrMn and CoFe layers were optimized to establish a strong exchange bias effect at the AF/FM interface. Magnetic annealing was performed to further enhance the exchange bias field. The Cu spacer thickness was tuned to achieve appreciable interlayer coupling between the pinned FM layer and the free FM layer. A combination of a thin pinned layer and a thick free layer was used to achieve high sensitivity, which is presumably associated with the spin collinear structures in ferromagnetic thin films.[76] The thin CoFe insertion layer works as a barrier against atomic diffusion during annealing and it also promotes spin-dependent scattering.[77]

Surface morphology of the nanoparticle-assembled film on spin valve was studied. The optical image in Figure 3a and the SEM image in Figure 3b both show that the nanoparticle-assembled film is uniform and continuous at different scales. It is noteworthy that the surface coverage of the nanoparticle-assembled film on the spin-valve thin films is very high (>94% in area), and this may benefit from the extensive purification, which was experimentally proved to facilitate the formation of uniform Langmuir film in our case.[67] The 2D AFM mapping in Figure 3c giving a root-mean-square roughness of 2.5 nm indicates that the flatness of the nanoparticle-assembled film was maintained after changing the deposition surface. Additionally, the cross-section profile (Figure 3d inset) extracted from the 3D AFM image at the film boundary (Figure 3d) reflects a film thickness of 41.8 ± 1.1 nm, which approximately corresponds to four layers of nanoparticles. The thickness of the nanoparticle-assembled film prepared on spin-valve surface differs from that prepared on Si surface, implying that the surface properties of the deposition surface influence the film thickness. Other experimental factors affecting the film thickness include evaporation rate of the organic carrier solvent, area of the liquid surface, dipping angle of the substrate, and concentration of the nanoparticle solution. Our experimental results suggest that the most effective way to control the film thickness is to modulate the nanoparticle solution concentration. For example, by reducing the nanoparticle solution concentration from 18 to 9 mg mL^{-1}, the estimated number of nanoparticle layers in the nanoparticle-assembled film was changed from four to two, and meanwhile dense and full substrate coverage was maintained. Besides,

DOI: 10.1021/acs.jpcc.7b07242
J. Phys. Chem. C 2017, 121, 22508−22516

given the close packing of the nanoparticles and the steep slope of the assembly front, it can be inferred that the nanoparticles were organized into multilayer structure. Unlike the highly ordered nanoparticle monolayer prepared by evaporation-induced self-assembly (Figure 2a,b), this nanoparticle-assembled multilayer film here did not exhibit long-range structural order; yet, they exhibited compact organization and close attachment on the sputtered thin films, which allow the investigation of their influence on the physical properties of the spin valve. On the other hand, the ability to tune the thickness of the nanoparticle-assembled film in the interfacial self-assembly method provides structural control for nanoparticle integration with surfaces or devices.

3.4. Magnetization Study. Magnetization study was performed by measuring the field-dependent magnetization curves (MH curves) of the spin-valve sample and the nanoparticle-integrated spin-valve sample. The high-field MH curves are presented in Figure 4a. It is observed that both

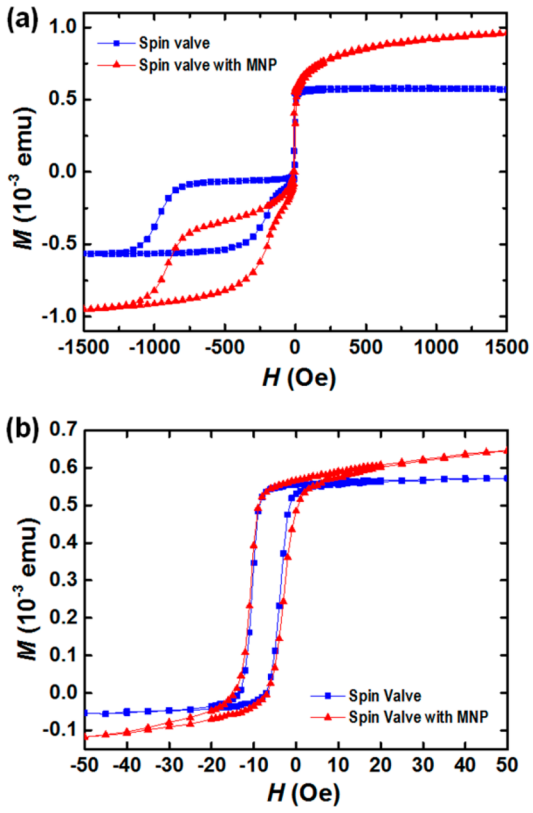

Figure 4. (a) High-field MH curve and (b) low-field MH curve of the spin valve (blue curve with squares) and the nanoparticle-integrated spin valve (red curve with triangles).

samples exhibited two separated hysteresis loops, which were related to the magnetizations of free layer and pinned layer. The free-layer magnetization dominated the MH curve at low field range, whereas the pinned-layer magnetization demonstrated obvious shift toward negative-field direction due to the established exchange-bias effect. The exchange-bias field (H_{ex}) and the pinned-layer coercivity ($H_{c\text{-pinned}}$) measured from the MH curve of the spin-valve sample are 586.2 ± 0.9 and 381.3 ± 0.6 Oe, respectively, confirming that strong exchange bias ($H_{ex} > H_{c\text{-pinned}}$) was achieved. Compared with the spin-valve sample, the nanoparticle-integrated spin-valve sample exhibited enlarged magnetization, which can be attributed to the nonlinear magnetization contribution from the nanoparticles at high field range. No discernible difference in pinned-layer coercivity and exchange-bias strength was found in these two samples. In order to finely evaluate the magnetization behavior of the free layer, the low-field magnetization curves of the two samples were measured and compared, and the results are presented in Figure 4b. In both samples, the free-layer hysteresis loop shifted to the same direction as that of the pinned layer case, and the offset of the free-layer magnetization switching was used to evaluate the interlayer coupling strength.[78] Without the presence of nanoparticles, the as-fabricated spin-valve sample exhibited free-layer coercivity ($H_{c\text{-free}}$) of 3.4 ± 0.1 Oe and interlayer coupling field (H_{int}) of 7.1 ± 0.1 Oe. After integrating the magnetic nanoparticles with the spin valve, the free-layer coercivity was increased asymmetrically, accompanied by the change of the interlayer coupling field. Note that the exact values of the free-layer coercivity and the interlayer coupling field in the nanoparticle-integrated sample cannot be directly extracted from the low field MH curve due to the distortion of the curve, which results from the magnetization contribution from the magnetic nanoparticles. These parameters were further evaluated and will be discussed in the following part regarding magnetoresistance analysis. Besides, the magnetization influence of the nanoparticles at low field range is relatively weak compared with the high field case.

3.5. Magnetoresistance Study. Magnetoresistance study was carried out by acquiring the field-dependent magnetoresistance curves (MR curves) of the spin-valve sample and the nanoparticle-integrated spin-valve sample. The major MR curves measured at high field range are shown in Figure 5a.

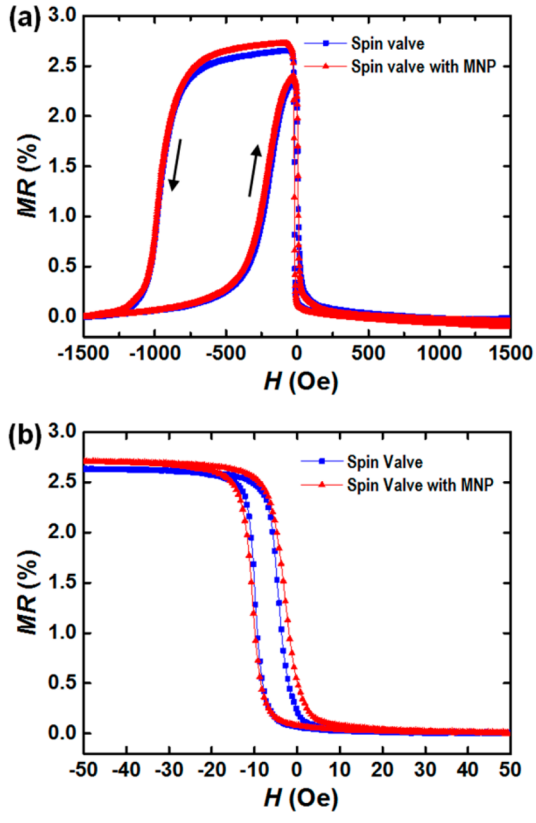

Figure 5. (a) Major MR curve and (b) minor MR curve of the spin valve (blue curve with squares) and the nanoparticle-integrated spin valve (red curve with triangles).

DOI: 10.1021/acs.jpcc.7b07242
J. Phys. Chem. C 2017, 121, 22508−22516

When magnetizing the two samples along the negative-field direction, the descending branch of the MR curve exhibited a plateau, indicating a large region of antiparallel magnetization configuration between the free layer and pinned layer.[7] When demagnetizing the two samples along the positive-field direction, a sharp peak was observed in the ascending branch of the MR curve, suggesting that the antiparallel magnetization configuration only occurred within a narrow region, which can be ascribed to the large coercivity and the gradual magnetization reversal of the pinned layer.[7,79] Note that the variations in grain size, interface coupling, and stress must be considered in the sputtered thin films. These factors gave rise to the disordered AF/FM interface moment and the distribution of antiferromagnetic anisotropy, as manifested by the rounded shape of the pinned-layer MR curves.[78] By comparison, it is observed that the nanoparticle-integrated spin-valve sample exhibited nearly the same values of pinned-layer coercivity and exchange-bias field as those of the spin-valve sample (578.4 ± 0.9 and 379.7 ± 0.7 Oe), indicating that the introduction of nanoparticles in the spin valve did not alter the pinned-layer coercivity or the exchange-bias strength. Such results match with the magnetization measurements in Figure 4a. Here the MR ratio is defined as $(R_{ap} - R_p)/R_p$, where R_p and R_{ap} are the resistance of parallel and antiparallel magnetization configurations, respectively. It is noteworthy that a slight increase of the MR ratio is observed in the major MR curve of the nanoparticle-integrated spin-valve sample. To accurately evaluate the change of the MR ratio and also study the magnetoresistance behaviors of the free layer, the minor MR curves of the two samples were measured at low field range and the results are presented in Figure 5b. By integrating the nanoparticles with spin valve, the MR ratio was increased from 2.64 ± 0.01% to 2.71 ± 0.01%, approximately corresponding to an enhancement of 0.07%. In addition, the free-layer coercivity measured from the MR curves was increased from 2.7 ± 0.1 to 3.9 ± 0.1 Oe, which confirms the change of free-layer coercivity as observed in the MH curves in Figure 4b. Interestingly, the interlayer coupling field, measured as the offset of free-layer MR curve from the zero-field axis, was reduced from 7.0 ± 0.2 to 6.6 ± 0.2 Oe, and this suggests that the integrated magnetic nanoparticles influenced the magnetization process of the free layer and hence affected the interlayer coupling between the free layer and the pinned layer. Overall, the magnetoresistance analysis complements the magnetization analysis by providing accurate evaluations of the exchange-bias field, pinned- and free-layer coercivity, interlayer coupling field, and magnetoresistance performance.

3.6. Interaction between Nanoparticles and Spin Valve. On the basis of the characterization results of the nanoparticles and the measurement results of the spin valves, a mechanism explaining the interaction between the nanoparticle and the spin valve can be proposed. In our system, the nanoparticle-assembled multilayer film was densely deposited on the surface of the bottom-pinned spin valve, as depicted in Figure 6. The spin valve exhibits weak interlayer coupling mediated by the spacer, and strong exchange bias effect at the AF/FM interface. As for the $CoFe_2O_4$ nanoparticles, they demonstrate single magnetic domain behavior due to the small size (10 nm) and their dipole moments show nearly linear response to the external magnetic field (H) at low field range (Figure 2d inset). Taking account of the thickness of the Ru capping layer (3 nm) in the spin valve and the thickness of the surfactants (~2 nm) capped on nanoparticle surface, the distance from the bottom of the nanoparticle to the top of the free layer can be approximated as 5 nm. Given the short distance between the nanoparticles and the free layer, the magnetic stray field generated from the magnetic nanoparticles further exerted on the free layer. This stray field induced by the nanoparticles is in the direction opposite to the free-layer magnetization. Consequently, the effective magnetic field applied on the free layer is reduced and the magnetization rotation process of the free layer is affected, as evidenced by the increase of free-layer coercivity. On the other hand, the free layer has a weak ferromagnetic coupling with the underneath pinned layer, since the MH curve and MR curve of the free layer shift slightly to the same direction as that of the pinned layer case. Generally, the interlayer coupling is considered as the superposition of the magnetostatic coupling (Néel orange-peel coupling), the pinhole coupling, and the oscillatory coupling (RKKY exchange interaction).[78] Given the composition and thickness of the spacer (Cu, 4 nm) in our spin valve, the ferromagnetic-type interlayer coupling here is presumably related to the magnetostatic coupling resulting from positively correlated waviness of the FM/spacer and spacer/FM interfaces.[62,78] Such interlayer coupling is weakened after introducing nanoparticles on spin valve surface, due to the decrease of the free-layer magnetization. Since the ferromagnetic-type interlayer coupling favors parallel magnetization configuration, the reduction of this interlayer coupling leads to the enhancement of antiparallel magnetization configuration, which is manifested by the increase of the MR ratio.

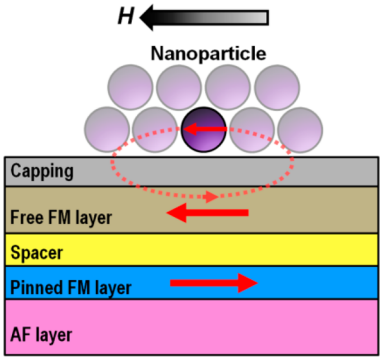

Figure 6. (a) Illustration of the magnetic interactions between the nanoparticle and the spin valve (not to scale). The red arrows represent the magnetization, H denotes the applied magnetic field, the dashed line indicates the stray field induced from the nanoparticle, and a high-resistance state of the spin valve is presented.

The results and the analysis above bring in the concept that independent control of the free-layer magnetization switching in spin-valve thin films can be achieved by introducing magnetic nanoparticles with appropriate organizations and properties. Furthermore, if the exchange-biased spin valve is fabricated with thinner spacer and thinner capping layer to induce stronger interlayer coupling and to improve its interaction with the nanoparticles, larger decrease of the interlayer coupling field and stronger enhancement of the MR ratio can be expected after nanoparticle integration. Note that the magnetization switching and magnetoresistance change of the spin valve occur at small field, where the nanoparticles acquire weak magnetic moments. If the nanoparticles are integrated into exchange-biased system with large operating field, significant improvement of the device performance can be anticipated. Further experiments will be performed to fabricate exchange-biased thin

DOI: 10.1021/acs.jpcc.7b07242
J. Phys. Chem. C 2017, 121, 22508−22516

film system with suitable configurations and explore its interaction with integrated magnetic nanoparticles by varying the capping-layer thickness.

4. CONCLUSION

In summary, this work reports the magnetization and magnetoresistance study of $CoFe_2O_4$ nanoparticle-integrated spin valve. By employing a modified interfacial self-assembly method, uniform thin films composed of monodisperse magnetic nanoparticles were produced. The formation of water/toluene interface and the control of liquid evaporation allow the preparation of nanoparticle-assembled film at large scale. This film was further transferred to Si substrate in a facile and fast manner without additional treatment. In a similar way, the nanoparticle-assembled film was deposited on the sputtered thin films of spin valve. Measurement results show that the integrated nanoparticles cause the decrease of interlayer coupling field and the increase of MR ratio in the spin valve. Further investigation of the interaction mechanism indicates that the magnetic stray field generated from the nanoparticles reduces the externally applied field on the free layer, leading to the change of free-layer magnetization, the attenuation of interlayer coupling strength, and the enhancement of magnetoresistance.

The presented fabrication procedures provide a facile route to integrate assembled magnetic nanoparticles with spin-valve thin films, enabling us to investigate their magnetic interactions at a range of several nanometers. Moreover, the ability to modulate the magnetization and magnetoresistance behaviors of spin valve by nanoparticle integration is beneficial for engineering spintronic devices with desired performance toward magnetic sensing and recording applications.

■ ASSOCIATED CONTENT

Supporting Information

The Supporting Information is available free of charge on the ACS Publications website at DOI: 10.1021/acs.jpcc.7b07242.

Optical image, SEM image, and AFM image of the $CoFe_2O_4$ nanoparticle-assembled film on Si substrate (PDF)

■ AUTHOR INFORMATION

Corresponding Author

*Tel: (+852) 2857 8491. E-mail: ppong@eee.hku.hk.

ORCID

Chengpeng Jiang: 0000-0003-4052-0804

Notes

The authors declare no competing financial interest.

■ ACKNOWLEDGMENTS

This research was supported by the Seed Funding Program for Basic Research, Seed Funding Program for Applied Research and Small Project Funding Program from University of Hong Kong, ITF Tier 3 funding (ITS-104/13, ITS-214/14), and University Grants Committee of Hong Kong (AoE/P-04/08). Xu Li (HKU) is thanked for helpful discussions. Theresa Ng (PolyU) is thanked for AFM experiments. C.W.L. acknowledges the support by PolyU (G-YBPU, 1-ZE25, 1-ZVGH).

■ REFERENCES

(1) Wu, M.; Aziz, A.; Witt, J.; Hickey, M.; Ali, M.; Marrows, C.; Hickey, B.; Blamire, M. Structural and Functional Analysis of Nanopillar Spin Electronic Devices Fabricated by 3D Focused Ion Beam Lithography. *Nanotechnology* **2008**, *19*, 485305.

(2) Kuo, T.-W.; Chen, P.-J.; Huang, H.-T.; Chen, M.-J.; Sheu, W.-J.; Hsieh, T.-F.; Chen, J.-Y.; Ouyang, H.; Wei, Z.-H. Wave-Like Pseudo-Spin Valve Thin Film as a Biosensor. *IEEE Trans. Magn.* **2014**, *50*, 1–3.

(3) Alayo, W.; Baggio-Saitovitch, E. Study of the Interlayer Coupling and Its Temperature Dependence in Spin Valves with Ru and Cu Spacers. *J. Appl. Phys.* **2010**, *107*, 073909.

(4) Nozieres, J.; Jaren, S.; Zhang, Y.; Zeltser, A.; Pentek, K.; Speriosu, V. Blocking Temperature Distribution and Long-Term Stability of Spin-Valve Structures with Mn-Based Antiferromagnets. *J. Appl. Phys.* **2000**, *87*, 3920–3925.

(5) Toney, M. F.; Samant, M. G.; Lin, T.; Mauri, D. Thickness Dependence of Exchange Bias and Structure in MnPt and MnNi Spin Valves. *Appl. Phys. Lett.* **2002**, *81*, 4565–4567.

(6) Childress, J.; Carey, M.; Wilson, R.; Smith, N.; Tsang, C.; Ho, M.; Carey, K.; MacDonald, S.; Ingall, L.; Gurney, B. IrMn Spin-Valves for High Density Recording. *IEEE Trans. Magn.* **2001**, *37*, 1745–1748.

(7) You, C.; Goripati, H.; Furubayashi, T.; Takahashi, Y.; Hono, K. Exchange Bias of Spin Valve Structure with a Top-Pinned $Co_{40}Fe_{40}B_{20}$/IrMn. *Appl. Phys. Lett.* **2008**, *93*, 012501.

(8) Kerr, E.; van Dijken, S.; Coey, J. Influence of the Annealing Field Strength on Exchange Bias and Magnetoresistance of Spin Valves with IrMn. *J. Appl. Phys.* **2005**, *97*, 093910.

(9) Rickart, M.; Guedes, A.; Franco, N.; Barradas, N.; Diaz, P.; MacKenzie, M.; Chapman, J.; Freitas, P. Exchange Bias in Ordered Antiferromagnets by Rapid Thermal Anneal without Magnetic Field. *J. Phys. D: Appl. Phys.* **2005**, *38*, 2151.

(10) Tanaka, A.; Shimizu, Y.; Seyama, Y.; Nagasaka, K.; Kondo, R.; Oshima, H.; Eguchi, S.; Kanai, H. Spin-Valve Heads in the Current-Perpendicular-to-Plane Mode for Ultrahigh-Density. Recording. *IEEE Trans. Magn.* **2002**, *38*, 84–88.

(11) Yuasa, H.; Kamiguchi, Y.; Sahashi, M. Dual Spin Valves with Nano-Oxide Layers. *J. Magn. Magn. Mater.* **2003**, *267*, 53–59.

(12) Yuasa, H.; Yoshikawa, M.; Kamiguchi, Y.; Koi, K.; Iwasaki, H.; Takagishi, M.; Sahashi, M. Output Enhancement of Spin-Valve Giant Magnetoresistance in Current-Perpendicular-to-Plane Geometry. *J. Appl. Phys.* **2002**, *92*, 2646–2650.

(13) Oshima, H.; Nagasaka, K.; Seyama, Y.; Jogo, A.; Shimizu, Y.; Tanaka, A.; Miura, Y. Current-Perpendicular Spin Valves with Partially Oxidized Magnetic Layers for Ultrahigh-Density Magnetic Recording. *IEEE Trans. Magn.* **2003**, *39*, 2377–2380.

(14) Leal, J.; Kryder, M. Spin Valves Exchange Biased by Co/Ru/Co Synthetic Antiferromagnets. *J. Appl. Phys.* **1998**, *83*, 3720–3723.

(15) Huai, Y.; Zhang, J.; Anderson, G.; Rana, P.; Funada, S.; Hung, C.-Y.; Zhao, M.; Tran, S. Spin-Valve Heads with Synthetic Antiferromagnet CoFe/Ru/CoFe/IrMn. *J. Appl. Phys.* **1999**, *85*, 5528–5530.

(16) Anderson, G.; Huai, Y.; Miloslawsky, L. CoFe/IrMn Exchange Biased Top, Bottom, and Dual Spin Valves. *J. Appl. Phys.* **2000**, *87*, 6989–6991.

(17) Jedema, F. J.; Filip, A. T.; van Wees, B. J. Electrical Spin Injection and Accumulation at Room Temperature in an All-Metal Mesoscopic Spin Valve. *Nature* **2001**, *410*, 345.

(18) Jedema, F. J.; Heersche, H. B.; Filip, A. T.; Baselmans, J. J. A.; van Wees, B. J. Electrical Detection of Spin Precession in a Metallic Mesoscopic Spin Valve. *Nature* **2002**, *416*, 713–716.

(19) Ambrose, T.; Liu, K.; Chien, C. Doubly Exchange-Biased NiCoO/NiFe/Cu/NiFe/NiCoO Spin Valves. *J. Appl. Phys.* **1999**, *85*, 6124–6126.

(20) Tehrani, S.; Slaughter, J. M.; Deherrera, M.; Engel, B. N.; Rizzo, N. D.; Salter, J.; Durlam, M.; Dave, R. W.; Janesky, J.; Butcher, B.; et al. Magnetoresistive Random Access Memory Using Magnetic Tunnel Junctions. *Proc. IEEE* **2003**, *91*, 703–714.

DOI: 10.1021/acs.jpcc.7b07242
J. Phys. Chem. C 2017, 121, 22508–22516

(21) Ikeda, S.; Hayakawa, J.; Lee, Y. M.; Matsukura, F.; Ohno, Y.; Hanyu, T.; Ohno, H. Magnetic Tunnel Junctions for Spintronic Memories and Beyond. *IEEE Trans. Electron Devices* **2007**, *54*, 991−1002.
(22) Yuasa, S.; Nagahama, T.; Fukushima, A.; Suzuki, Y.; Ando, K. Giant Room-Temperature Magnetoresistance in Single-Crystal Fe/MgO/Fe Magnetic Tunnel Junctions. *Nat. Mater.* **2004**, *3*, 868.
(23) Singh, A. K.; Eom, J. Negative Magnetoresistance in a Vertical Single-Layer Graphene Spin Valve at Room Temperature. *ACS Appl. Mater. Interfaces* **2014**, *6*, 2493−2496.
(24) Cobas, E.; Friedman, A. L.; van't Erve, O. M.; Robinson, J. T.; Jonker, B. T. Graphene as a Tunnel Barrier: Graphene-Based Magnetic Tunnel Junctions. *Nano Lett.* **2012**, *12*, 3000−3004.
(25) Zhou, J.; Wang, L.; Qin, R.; Zheng, J.; Mei, W. N.; Dowben, P.; Nagase, S.; Gao, Z.; Lu, J. Structure and Electronic and Transport Properties of Transition Metal Intercalated Graphene and Graphene-Hexagonal-Boron-Nitride Bilayer. *J. Phys. Chem. C* **2011**, *115*, 25273−25280.
(26) Wang, W.; Narayan, A.; Tang, L.; Dolui, K.; Liu, Y.; Yuan, X.; Jin, Y.; Wu, Y.; Rungger, I.; Sanvito, S.; et al. Spin-Valve Effect in NiFe/MoS_2/NiFe Junctions. *Nano Lett.* **2015**, *15*, 5261−5267.
(27) Jang, H. J.; Richter, C. A. Organic Spin-Valves and Beyond: Spin Injection and Transport in Organic Semiconductors and the Effect of Interfacial Engineering. *Adv. Mater.* **2017**, *29*, 1602739.
(28) Sun, D.; Ehrenfreund, E.; Vardeny, Z. V. The First Decade of Organic Spintronics Research. *Chem. Commun.* **2014**, *50*, 1781−1793.
(29) Wang, F.; Vardeny, Z. V. Organic Spin Valves: The First Organic Spintronics Devices. *J. Mater. Chem.* **2009**, *19*, 1685−1690.
(30) Singamaneni, S.; Bliznyuk, V. N.; Binek, C.; Tsymbal, E. Y. Magnetic Nanoparticles: Recent Advances in Synthesis, Self-Assembly and Applications. *J. Mater. Chem.* **2011**, *21*, 16819−16845.
(31) Dempsey, K.; Hindmarch, A.; Wei, H.-X.; Qin, Q.-H.; Wen, Z.-C.; Wang, W.-X.; Vallejo-Fernandez, G.; Arena, D.; Han, X.-F.; Marrows, C. Cotunneling Enhancement of Magnetoresistance in Double Magnetic Tunnel Junctions with Embedded Superparamagnetic NiFe Nanoparticles. *Phys. Rev. B: Condens. Matter Mater. Phys.* **2010**, *82*, 214415.
(32) Wu, L.; Jubert, P.-O.; Berman, D.; Imaino, W.; Nelson, A.; Zhu, H.; Zhang, S.; Sun, S. Monolayer Assembly of Ferrimagnetic $Co_xFe_{3-x}O4$ Nanocubes for Magnetic Recording. *Nano Lett.* **2014**, *14*, 3395−3399.
(33) Inomata, K.; Saito, Y. Spin-Dependent Tunneling through Layered Ferromagnetic Nanoparticles. *Appl. Phys. Lett.* **1998**, *73*, 1143−1145.
(34) Chapline, M. G.; Wang, S. X. Room-Temperature Spin Filtering in a $CoFe_2O_4/MgAl_2O_4/Fe_3O_4$ Magnetic Tunnel Barrier. *Phys. Rev. B: Condens. Matter Mater. Phys.* **2006**, *74*, 014418.
(35) Lekshmi, I. C.; Buonsanti, R.; Nobile, C.; Rinaldi, R.; Cozzoli, P. D.; Maruccio, G. Tunneling Magnetoresistance with Sign Inversion in Junctions Based on Iron Oxide Nanocrystal Superlattices. *ACS Nano* **2011**, *5*, 1731−1738.
(36) Wu, L.; Mendoza-Garcia, A.; Li, Q.; Sun, S. Organic Phase Syntheses of Magnetic Nanoparticles and Their Applications. *Chem. Rev.* **2016**, *116*, 10473−10512.
(37) Zeng, H.; Sun, S. Syntheses, Properties, and Potential Applications of Multicomponent Magnetic Nanoparticles. *Adv. Funct. Mater.* **2008**, *18*, 391−400.
(38) Jiang, C.; Leung, C. W.; Pong, P. W. Self-Assembled Thin Films of Fe_3O_4-Ag Composite Nanoparticles for Spintronic Applications. *Appl. Surf. Sci.* **2017**, *419*, 692−696.
(39) Yakushiji, K.; Ernult, F.; Imamura, H.; Yamane, K.; Mitani, S.; Takanashi, K.; Takahashi, S.; Maekawa, S.; Fujimori, H. Enhanced Spin Accumulation and Novel Magnetotransport in Nanoparticles. *Nat. Mater.* **2004**, *4*, 57.
(40) Song, Q.; Zhang, Z. J. Shape Control and Associated Magnetic Properties of Spinel Cobalt Ferrite Nanocrystals. *J. Am. Chem. Soc.* **2004**, *126*, 6164−6168.
(41) Bellido, E.; Domingo, N.; Ojea-Jiménez, I.; Ruiz-Molina, D. Structuration and Integration of Magnetic Nanoparticles on Surfaces and Devices. *Small* **2012**, *8*, 1465−1491.
(42) Wen, T.; Zhang, D.; Wen, Q.; Zhang, H.; Liao, Y.; Li, Q.; Yang, Q.; Bai, F.; Zhong, Z. Magnetic Nanoparticle Assembly Arrays Prepared by Hierarchical Self-Assembly on a Patterned Surface. *Nanoscale* **2015**, *7*, 4906−4911.
(43) Park, J.-I.; Jun, Y.-w.; Choi, J.-s.; Cheon, J. Highly Crystalline Anisotropic Superstructures Via Magnetic Field Induced Nanoparticle Assembly. *Chem. Commun.* **2007**, 5001−5003.
(44) Pichon, B. P.; Leuvey, C.; Ihawakrim, D.; Bernard, P.; Schmerber, G.; Begin-Colin, S. Magnetic Properties of Mono-and Multilayer Assemblies of Iron Oxide Nanoparticles Promoted by Sams. *J. Phys. Chem. C* **2014**, *118*, 3828−3837.
(45) Pichon, B. t. P.; Demortière, A.; Pauly, M.; Mougin, K.; Derory, A.; Bégin-Colin, S. 2D Assembling of Magnetic Iron Oxide Nanoparticles Promoted by SAMs Used as Well-Addressed Surfaces. *J. Phys. Chem. C* **2010**, *114*, 9041−9048.
(46) Dong, A.; Chen, J.; Vora, P. M.; Kikkawa, J. M.; Murray, C. B. Binary Nanocrystal Superlattice Membranes Self-Assembled at the Liquid-Air Interface. *Nature* **2010**, *466*, 474.
(47) Wen, T.; Majetich, S. A. Ultra-Large-Area Self-Assembled Monolayers of Nanoparticles. *ACS Nano* **2011**, *5*, 8868−8876.
(48) Pauly, M.; Pichon, B. P.; Albouy, P.-A.; Fleutot, S.; Leuvrey, C.; Trassin, M.; Gallani, J.-L.; Begin-Colin, S. Monolayer and Multilayer Assemblies of Spherically and Cubic-Shaped Iron Oxide Nanoparticles. *J. Mater. Chem.* **2011**, *21*, 16018−16027.
(49) Fleutot, S.; Nealon, G. L.; Pauly, M.; Pichon, B. P.; Leuvrey, C.; Drillon, M.; Gallani, J.-L.; Guillon, D.; Donnio, B.; Bégin-Colin, S. Spacing-Dependent Dipolar Interactions in Dendronized Magnetic Iron Oxide Nanoparticle 2D Arrays and Powders. *Nanoscale* **2013**, *5*, 1507−1516.
(50) Yan, C.; Wang, T. A New View for Nanoparticle Assemblies: From Crystalline to Binary Cooperative Complementarity. *Chem. Soc. Rev.* **2017**, *46*, 1483−1509.
(51) Kinge, S.; Crego-Calama, M.; Reinhoudt, D. N. Self-Assembling Nanoparticles at Surfaces and Interfaces. *ChemPhysChem* **2008**, *9*, 20−42.
(52) Devasahayam, A.; Sides, P.; Kryder, M. Magnetic, Temperature, and Corrosion Properties of the Nife/Irmn Exchange Couple. *J. Appl. Phys.* **1998**, *83*, 7216−7218.
(53) Sun, S.; Zeng, H.; Robinson, D. B.; Raoux, S.; Rice, P. M.; Wang, S. X.; Li, G. Monodisperse MFe_2O_4 (M = Fe, Co, Mn) Nanoparticles. *J. Am. Chem. Soc.* **2004**, *126*, 273−279.
(54) Chechenin, N.; Chernykh, P.; Dushenko, S.; Dzhun, I.; Goikhman, A.; Rodionova, V. Asymmetry of Magnetization Reversal of Pinned Layer in NiFe/Cu/NiFe/IrMn Spin-Valve Structure. *J. Supercond. Novel Magn.* **2014**, *27*, 1547−1552.
(55) Ali, M.; Marrows, C.; Hickey, B. Onset of Exchange Bias in Ultrathin Antiferromagnetic Layers. *Phys. Rev. B: Condens. Matter Mater. Phys.* **2003**, *67*, 172405.
(56) Aley, N.; Vallejo-Fernandez, G.; Kroeger, R.; Lafferty, B.; Agnew, J.; Lu, Y.; O'Grady, K. Texture Effects in IrMn/CoFe Exchange Bias Systems. *IEEE Trans. Magn.* **2008**, *44*, 2820−2823.
(57) Xie, J.; Peng, S.; Brower, N.; Pourmand, N.; Wang, S. X.; Sun, S. One-Pot Synthesis of Monodisperse Iron Oxide Nanoparticles for Potential Biomedical Applications. *Pure Appl. Chem.* **2006**, *78*, 1003−1014.
(58) Douglas, F. J.; MacLaren, D. A.; Murrie, M. A Study of the Role of the Solvent During Magnetite Nanoparticle Synthesis: Tuning Size, Shape and Self-Assembly. *RSC Adv.* **2012**, *2*, 8027−8035.
(59) Jiang, C.; Leung, C. W.; Pong, P. W. Magnetic-Field-Assisted Assembly of Anisotropic Superstructures by Iron Oxide Nanoparticles and Their Enhanced Magnetism. *Nanoscale Res. Lett.* **2016**, *11*, 189.
(60) Sathya, A.; Guardia, P.; Brescia, R.; Silvestri, N.; Pugliese, G.; Nitti, S.; Manna, L.; Pellegrino, T. $Co_xFe_{3-x}O_4$ Nanocubes for Theranostic Applications: Effect of Cobalt Content and Particle Size. *Chem. Mater.* **2016**, *28*, 1769−1780.

DOI: 10.1021/acs.jpcc.7b07242
J. Phys. Chem. C 2017, 121, 22508−22516

(61) López-Ortega, A.; Lottini, E.; Fernandez, C. d. J.; Sangregorio, C. Exploring the Magnetic Properties of Cobalt-Ferrite Nanoparticles for the Development of a Rare-Earth-Free Permanent Magnet. *Chem. Mater.* **2015**, *27*, 4048−4056.
(62) Jiang, C.; Ng, S. M.; Leung, C. W.; Pong, P. W. Magnetically Assembled Iron Oxide Nanoparticle Coatings and Their Integration with Pseudo-Spin-Valve Thin Films. *J. Mater. Chem. C* **2017**, *5*, 252−263.
(63) Disch, S.; Wetterskog, E.; Hermann, R. P.; Salazar-Alvarez, G.; Busch, P.; Brückel, T.; Bergström, L.; Kamali, S. Shape Induced Symmetry in Self-Assembled Mesocrystals of Iron Oxide Nanocubes. *Nano Lett.* **2011**, *11*, 1651−1656.
(64) Ye, X.; Collins, J. E.; Kang, Y.; Chen, J.; Chen, D. T.; Yodh, A. G.; Murray, C. B. Morphologically Controlled Synthesis of Colloidal Upconversion Nanophosphors and Their Shape-Directed Self-Assembly. *Proc. Natl. Acad. Sci. U. S. A.* **2010**, *107*, 22430−22435.
(65) Shevchenko, E. V.; Talapin, D. V.; Kotov, N. A.; O'brien, S.; Murray, C. B. Structural Diversity in Binary Nanoparticle Superlattices. *Nature* **2006**, *439*, 55.
(66) Debnath, B.; Bansal, A.; Salunke, H. G.; Sadhu, A.; Bhattacharyya, S. Enhancement of Magnetization through Interface Exchange Interactions of Confined NiO Nanoparticles within the Mesopores of $CoFe_2O_4$. *J. Phys. Chem. C* **2016**, *120*, 5523−5533.
(67) Aleksandrovic, V.; Greshnykh, D.; Randjelovic, I.; Fromsdorf, A.; Kornowski, A.; Roth, S. V.; Klinke, C.; Weller, H. Preparation and Electrical Properties of Cobalt−Platinum Nanoparticle Monolayers Deposited by the Langmuir−Blodgett Technique. *ACS Nano* **2008**, *2*, 1123−1130.
(68) Giner-Casares, J. J.; Reguera, J. Directed Self-Assembly of Inorganic Nanoparticles at Air/Liquid Interfaces. *Nanoscale* **2016**, *8*, 16589−16595.
(69) Booth, S. G.; Dryfe, R. A. Assembly of Nanoscale Objects at the Liquid/Liquid Interface. *J. Phys. Chem. C* **2015**, *119*, 23295−23309.
(70) Confalonieri, G. A. B.; Szary, P.; Mishra, D.; Benitez, M. J.; Feyen, M.; Lu, A. H.; Agudo, L.; Eggeler, G.; Petracic, O.; Zabel, H. Magnetic Coupling Mechanisms in Particle/Thin Film Composite Systems. *Beilstein J. Nanotechnol.* **2010**, *1*, 101.
(71) Useinov, A.; Ye, L.-X.; Useinov, N.; Wu, T.-H.; Lai, C.-H. Anomalous Tunnel Magnetoresistance and Spin Transfer Torque in Magnetic Tunnel Junctions with Embedded Nanoparticles. *Sci. Rep.* **2015**, *5*, 18026.
(72) Li, G.; Sun, S.; Wilson, R. J.; White, R. L.; Pourmand, N.; Wang, S. X. Spin Valve Sensors for Ultrasensitive Detection of Superparamagnetic Nanoparticles for Biological Applications. *Sens. Actuators, A* **2006**, *126*, 98−106.
(73) Graham, D.; Ferreira, H.; Feliciano, N.; Freitas, P.; Clarke, L.; Amaral, M. Magnetic Field-Assisted DNA Hybridisation and Simultaneous Detection Using Micron-Sized Spin-Valve Sensors and Magnetic Nanoparticles. *Sens. Actuators, B* **2005**, *107*, 936−944.
(74) Tamanaha, C.; Mulvaney, S.; Rife, J.; Whitman, L. Magnetic Labeling, Detection, and System Integration. *Biosens. Bioelectron.* **2008**, *24*, 1−13.
(75) Gaster, R. S.; Xu, L.; Han, S.-J.; Wilson, R. J.; Hall, D. A.; Osterfeld, S. J.; Yu, H.; Wang, S. X. Quantification of Protein Interactions and Solution Transport Using High-Density GMR Sensor Arrays. *Nat. Nanotechnol.* **2011**, *6*, 314−320.
(76) Tu, B. D.; Danh, T. M.; Duc, N. H.; et al. Optimization of Planar Hall Effect Sensor for Magnetic Bead Detection Using Spin-Valve NiFe/Cu/NiFe/IrMn Structures. *J. Phys.: Conf. Ser.* **2009**, *187*, 012056.
(77) Parkin, S. Origin of Enhanced Magnetoresistance of Magnetic Multilayers: Spin-Dependent Scattering from Magnetic Interface States. *Phys. Rev. Lett.* **1993**, *71*, 1641.
(78) Alayo, W.; Xing, Y.; Baggio-Saitovitch, E. Magnetization Studies in IrMn/Co/Ru/NiFe Spin Valves with Weak Interlayer Coupling. *J. Appl. Phys.* **2009**, *106*, 113903.
(79) Fulara, H.; Chaudhary, S.; Kashyap, S. C. Interdependence of Reversal Asymmetry and Training Effect in $Ir_{22}Mn_{78}/Ni_{81}Fe_{19}$ Bilayers Probed with Magnetoresistance. *Appl. Phys. Lett.* **2012**, *101*, 142408.

DOI: 10.1021/acs.jpcc.7b07242
J. Phys. Chem. C 2017, 121, 22508−22516